

Carnegie Mellon
Software Engineering Institute

A Case Study on Analytical Analysis of the Inverted Pendulum Real-Time Control System

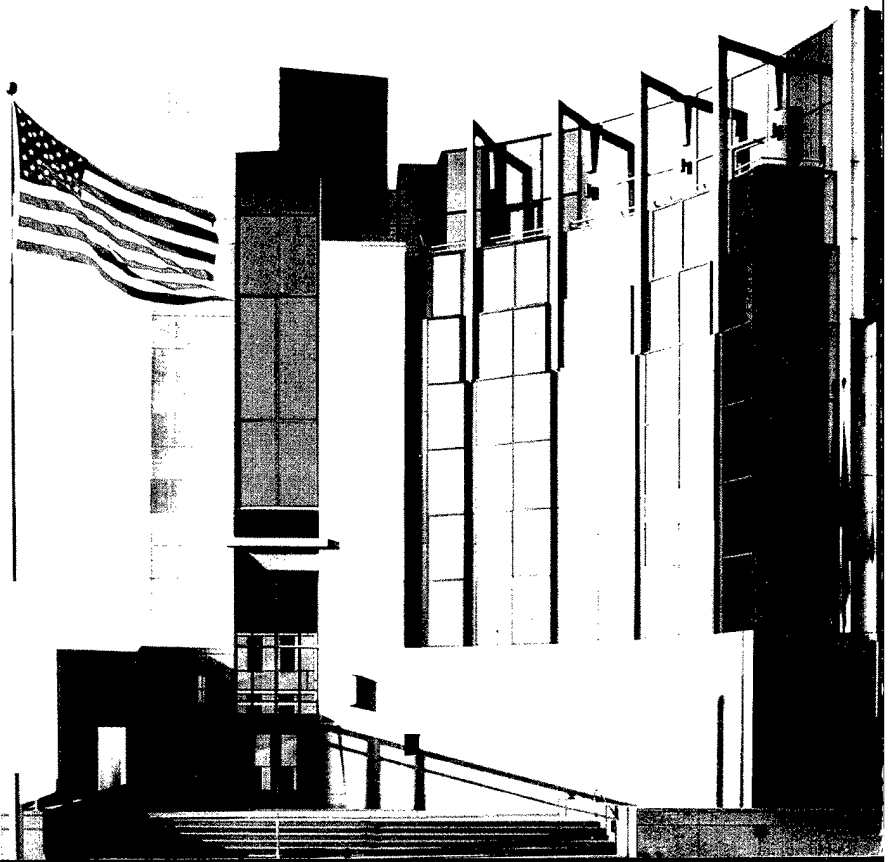
Danbing Seto
Lui Sha

November 1999

TECHNICAL REPORT
CMU/SEI-99-TR-023
ESC-TR-99-023

DISTRIBUTION STATEMENT A
Approved for Public Release
Distribution Unlimited

20000204 133





Carnegie Mellon
Software Engineering Institute
Pittsburgh, PA 15213-3890

A Case Study on Analytical Analysis of the Inverted Pendulum Real-Time Control System

CMU/SEI-99-TR-023
ESC-TR-99-023

Danbing Seto
Lui Sha

October 1999

Dependable System Upgrade

Unlimited distribution subject to the copyright.

DTIC QUALITY INSPECTED 1

This report was prepared for the

SEI Joint Program Office
HQ ESC/DIB
5 Eglin Street
Hanscom AFB, MA 01731-2116

The ideas and findings in this report should not be construed as an official DoD position. It is published in the interest of scientific and technical information exchange.

FOR THE COMMANDER



Norton L. Compton, Lt Col., USAF
SEI Joint Program Office

This work is sponsored by the U.S. Department of Defense. The Software Engineering Institute is a federally funded research and development center sponsored by the U.S. Department of Defense.

Copyright 1999 by Carnegie Mellon University.

NO WARRANTY

THIS CARNEGIE MELLON UNIVERSITY AND SOFTWARE ENGINEERING INSTITUTE MATERIAL IS FURNISHED ON AN "AS-IS" BASIS. CARNEGIE MELLON UNIVERSITY MAKES NO WARRANTIES OF ANY KIND, EITHER EXPRESSED OR IMPLIED, AS TO ANY MATTER INCLUDING, BUT NOT LIMITED TO, WARRANTY OF FITNESS FOR PURPOSE OR MERCHANTABILITY, EXCLUSIVITY, OR RESULTS OBTAINED FROM USE OF THE MATERIAL. CARNEGIE MELLON UNIVERSITY DOES NOT MAKE ANY WARRANTY OF ANY KIND WITH RESPECT TO FREEDOM FROM PATENT, TRADEMARK, OR COPYRIGHT INFRINGEMENT.

Use of any trademarks in this report is not intended in any way to infringe on the rights of the trademark holder.

Internal use. Permission to reproduce this document and to prepare derivative works from this document for internal use is granted, provided the copyright and "No Warranty" statements are included with all reproductions and derivative works.

External use. Requests for permission to reproduce this document or prepare derivative works of this document for external and commercial use should be addressed to the SEI Licensing Agent.

This work was created in the performance of Federal Government Contract Number F19628-95-C-0003 with Carnegie Mellon University for the operation of the Software Engineering Institute, a federally funded research and development center. The Government of the United States has a royalty-free government-purpose license to use, duplicate, or disclose the work, in whole or in part and in any manner, and to have or permit others to do so, for government purposes pursuant to the copyright license under the clause at 52.227-7013.

For information about purchasing paper copies of SEI reports, please visit the publications portion of our Web site (<http://www.sei.cmu.edu/publications/pubweb.html>).

Table of Contents

Abstract	vii
1 Introduction	1
2 An Analytic Model of Inverted Pendulum System	3
3 Feedback Control Design and Implementation	7
3.1 Controller Design and System Performance	8
3.2 Stability Regions	11
3.3 Controller Implementation	16
4 Design of Control Switching Logic	21
4.1 Safety Region and Safety of the Physical System	21
4.2 Design of Control Switching Logic	23
5 Conclusions	29
References	33
Appendix A	35
A1 Performance Evaluation	35
A2 Stability Region of Linear Control Systems with Linear Constraints	37
A3 Digitized Control Implementation	40
A4 Delay Caused by Digital Filter	40

List of Figures

Figure 1: An Inverted Pendulum Control System	1
Figure 2: A Small Portion of the Pendulum	3
Figure 3: Friction Model for the Cart	5
Figure 4: Simulation Result	10
Figure 5: The Largest Stability Region (with K_1 and K_2 projected to $x_1 \sim x_2$ phase plan and $x_3 \sim x_4$ phase plane)	13
Figure 6: The Largest Stability Region (with K variable, projected on $x_1 \sim x_2$ phase plan and $x_3 \sim x_4$ phase plane)	14
Figure 7: Performance Under Three Controllers	15
Figure 8: The Largest Stability Regions (projected to $x_1 \sim x_2$ phase plan and $x_3 \sim x_4$ phase plane)	15
Figure 9: Measurement Noises of Track Position and Pendulum	17
Figure 10: Track Position with Raw Measurement, Filtered Data, and Projected Data	19
Figure 11: Simulation Result	22
Figure 12: Check if the Physical System is Safe, and if it is Ready for Baseline Control	23
Figure 13: Application Controller State Transition Diagram	24
Figure 14: Active Controller State Transition Diagram	25
Figure 15: Illustration of Tolerating a Fault Caused by a Brute Force Bug	26
Figure 16: Lyapunov Function Values	27
Figure 17: Linear Transformations Between the Physical Position of the Variable and the Ticks (cart position: $0.004365 * \text{ticks}$; angle: $0.0359 * \text{ticks}$)	30
Figure 18: Measures for the Transient Response of $x(t)$	36
Figure 19: (a) Number of Sampling Periods Delayed as a Function of the Signal Frequency (b) Signals Before and After Filtering	42

List of Tables

Table 1: Performance Measures of the Closed-Loop System with V_{a1} and V_{a2}	11
Table 2: Summary of the Comparison on Performance and Stability Region of Three Different Controllers	16

Abstract

An inverted pendulum has been used as the controlled device in a prototype real-time control system employing the SimplexTM architecture. In this report, we address the control issues of such a system in an analytic way. In particular, an analytic model of the system is derived; control algorithms are designed for the baseline control, experimental control and safety control based on the concept of analytic redundancy; the safety region is obtained as the stability region of the system under the safety control; and the control switching logic is established to provide fault tolerant functionality. Finally, the results obtained and the lessons learned are summarized, and future work is discussed.

TM Simplex is a trademark of Carnegie Mellon University.

1 Introduction

An inverted pendulum has been used as a controlled device in a prototype control system employing the Simplex architecture. As shown in Figure 1, the physical system consists of a cart, driven by a DC motor, and a pendulum attached to the cart. The cart can move along a horizontal track, and the pendulum is able to rotate freely in the range of $[-30^\circ, 30^\circ]$ with respect to vertical in the vertical plane parallel to the track. There is no direct control applied to the pendulum. Both the position of the cart x and the angle θ are measurable through two potentiometers. The dynamics of the system are described by the state of the system, which consists of the cart position x , the cart velocity \dot{x} , the pendulum angle θ , and the pendulum angular velocity $\dot{\theta}$. The physical system has state and control constraints. Specifically, the cart position is restricted in the range $[-0.7, 0.7]$ meters, the maximum speed of the cart is 1.0 meter/second, the angle is constrained to the range $[-30^\circ, 30^\circ]$, and the motor input voltage is limited in the range $[-4.96, 4.96]$ volts.

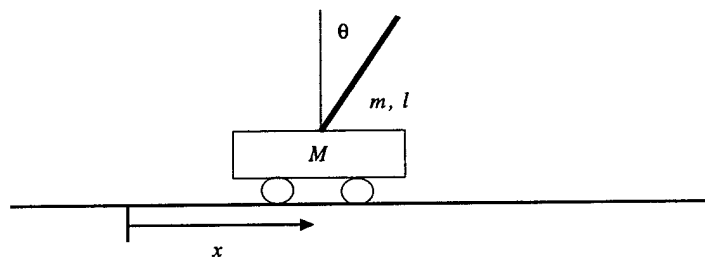


Figure 1: An Inverted Pendulum Control System

The control objective of the inverted pendulum system is to move the cart from one position to another along the track with the pendulum standing still at the upright position, i.e., $\theta \approx 0$. Since the equilibrium at $\theta = 0$ is unstable, such control objective has to be achieved while maintaining the stability of the system. As the DC motor has only limited power and the track has finite length, there exist certain states of the physical system from which the pendulum cannot be steered back to the upright position. Therefore, the notion of a safety region will be introduced to characterize a subset of the system state from which the system stability can always be maintained.

The report is organized as follows. In Section 2, we derive an analytic model for the inverted pendulum control system. In Section 3, the control system's primary objective of stabilization is presented and the notion of analytically redundant controllers is defined. Control algorithms are designed for the baseline controller, the experimental controller, and the safety controller based on the concept of analytic redundancy in the sense that all the controllers

will achieve the control objective, but they will result in different system performance and stability regions. Practical issues in the implementation of the controllers are discussed. In Section 4, the safety region is defined and the safety criterion of the physical system is described. A control switching logic is established to tolerate the timing and semantic faults. The report is concluded in Section 5 with discussions of the lessons learned and future work on real-time control systems employing the Simplex architecture.

2 An Analytic Model of Inverted Pendulum System

A complete analytic model of the inverted pendulum controlled by a DC motor is derived in three parts, the pendulum-cart dynamics, the friction model, and the motor dynamics. Details are given below.

Pendulum-cart dynamics: Euler-Lagrange Equation

Let M and m be the masses of the cart and pendulum, l be the length of the pendulum, F be the motor force applied to the cart, and f_c and f_p are the friction on the cart and on the pendulum, respectively. The kinetic energy of the cart is $K_c = M\dot{x}^2/2$ and the potential energy of the cart is zero with respect to a properly chosen reference. For the pendulum, consider a small portion with mass dm located at $q \in [0, l]$ as shown in Figure 2.

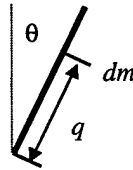


Figure 2: A Small Portion of the Pendulum

Then we have

$$\begin{cases} x_{dm} = x + q \sin \theta \\ y_{dm} = q \cos \theta \end{cases} \Rightarrow \begin{cases} \dot{x}_{dm} = \dot{x} + q \cos \theta \dot{\theta} \\ \dot{y}_{dm} = -q \sin \theta \dot{\theta} \end{cases}$$

kinetic energy of dm :

$$K_{dm} = \frac{1}{2} dm (\dot{x}_{dm}^2 + \dot{y}_{dm}^2) = \frac{1}{2} dm (\dot{x}^2 + 2q \cos \theta \dot{x} \dot{\theta} + q^2 \dot{\theta}^2)$$

and the potential energy of dm :

$$P_{dm} = dm g q \cos \theta$$

where $dm = \rho dq$ and ρ is the mass per unit length of the pendulum. The total kinetic energy and potential energy of the pendulum can be obtained by integrating K_{dm} and P_{dm} from 0 to l . Doing so, we obtain the total kinetic energy K and the potential energy P of the overall system given by

$$K = K_c + K_p = \frac{1}{2}(M + m)\dot{x}^2 + \frac{1}{2}ml \cos \theta \dot{x} \dot{\theta} + \frac{1}{6}ml^2 \dot{\theta}^2, \quad P = \frac{1}{2}mgl \cos \theta$$

and the resulting Lagrangian:

$$L = K - P = \frac{1}{2}(M + m)\dot{x}^2 + \frac{1}{2}ml \cos \theta \dot{x} \dot{\theta} + \frac{1}{6}ml^2 \dot{\theta}^2 - \frac{1}{2}mgl \cos \theta$$

Then the Euler-Lagrange equations

$$\frac{d}{dt} \frac{\partial L}{\partial \dot{x}} - \frac{\partial L}{\partial x} = F - f_c, \quad \frac{d}{dt} \frac{\partial L}{\partial \dot{\theta}} - \frac{\partial L}{\partial \theta} = -f_p$$

yield the equations of motion:

$$\begin{cases} (m + M)\ddot{x} + \frac{1}{2}ml \cos \theta \ddot{\theta} - \frac{1}{2}ml \sin \theta \dot{\theta}^2 = F - f_c \\ \frac{1}{2}ml \cos \theta \ddot{x} + \frac{1}{3}ml^2 \ddot{\theta} - \frac{1}{2}mgl \sin \theta = -f_p \end{cases} \quad (1)$$

Friction Model

We assume that both static friction and viscosity friction act on the cart and the pendulum joint. These frictions are described by the following functions:

$$f_c = \text{sgn}(\dot{x})A_x e^{-C_x |\dot{x}|} + B_x \dot{x}, \quad f_p = \text{sgn}(\dot{\theta})A_\theta e^{-C_\theta |\dot{\theta}|} + B_\theta \dot{\theta} \quad (2)$$

with $A_x, B_x, C_x, A_\theta, B_\theta, C_\theta > 0$. Friction f_c is depicted in Figure 3.

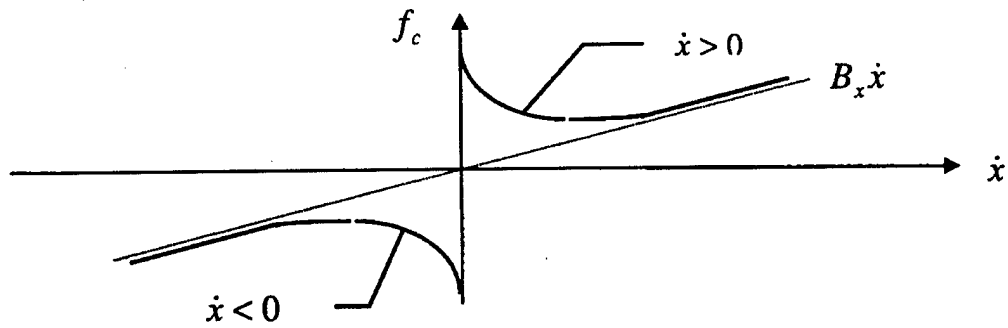


Figure 3: Friction Model for the Cart

Motor Dynamics

The dynamics of the DC motor are governed by the following equations:

$$\begin{aligned} L_a \dot{I}_a &= V_a - R_a I_a - E_b, \quad E_b = K_b \omega \\ J_m \dot{\omega} &= T_m - T_l - B_m \omega \end{aligned}$$

with the relations

$$T_m = K_i K_g I_a, T_l = Fr, \quad \omega = K_g \dot{x} / r$$

where

L_a - armature inductance	T_m - motor torque (no load)	K_i - torque constant
R_a - armature resistance	T_l - load torque	K_b - back-emf constant
I_a - armature current	ω - motor angular velocity	K_g - gear ratio
r - driving wheel radius	J_m - rotor inertia of motor	E_b - back emf.
V_a - armature voltage	B_m - viscous friction coefficient	F - force to the cart

Then the motor dynamics can be expressed in terms of I_a , x , and force F as

$$\begin{cases} L_a \dot{I}_a + R_a I_a + \frac{K_g K_b}{r} \dot{x} = V_a \\ \frac{K_g J_m}{r^2} \ddot{x} + \frac{K_g B_m}{r^2} \dot{x} - \frac{K_i K_g}{r} I_a = -F \end{cases} \quad (3)$$

Finally, by combining Eqs (1)-(3), we arrive at a complete model of the inverted pendulum control system with the control variable V_a :

$$\begin{cases} (m + M + \frac{K_g J_m}{r^2})\ddot{x} + \frac{1}{2}ml \cos \theta \ddot{\theta} + \frac{K_g B_m}{r^2} \dot{x} - \frac{K_g K_i}{r} I_a - \frac{1}{2}ml \sin \theta \dot{\theta}^2 = -f_c \\ \frac{1}{2}ml \cos \theta \ddot{x} + \frac{1}{3}ml^2 \ddot{\theta} - \frac{1}{2}mgl \sin \theta = -f_p \\ L_a \dot{I}_a + R_a I_a + \frac{K_g K_b}{r} \dot{x} = V_a \end{cases}$$

or

$$\begin{cases} \ddot{x} = \frac{1}{D} \left[-\frac{1}{3}ml^2(f_c + C_1) + \frac{1}{2}ml \cos \theta (f_p + C_2) \right] \\ \ddot{\theta} = \frac{1}{D} \left[\frac{1}{2}ml \cos \theta (f_c + C_1) - \overline{M}(f_p + C_2) \right] \\ \dot{I}_a = -\frac{R_a}{L_a} I_a - \frac{K_g K_b}{rL_a} \dot{x} + \frac{1}{L_a} V_a \end{cases} \quad (4)$$

where

$$\begin{aligned} f_c &= \text{sgn}(\dot{x}) A_x e^{-C_x |\dot{x}|} + B_x \dot{x}, & f_\theta &= \text{sgn}(\dot{\theta}) A_\theta e^{-C_\theta |\dot{\theta}|} + B_\theta \dot{\theta} \\ \overline{M} &= m + M + \frac{K_g J_m}{r^2}, & D &= \frac{1}{3} \overline{M} ml^2 - \frac{1}{4} m^2 l^2 \cos^2 \theta \\ C_1 &= \frac{K_g B_m}{r^2} \dot{x} - \frac{K_g K_i}{r} I_a - \frac{1}{2} ml \sin \theta \dot{\theta}^2, & C_2 &= -\frac{1}{2} mgl \sin \theta \end{aligned}$$

3 Feedback Control Design and Implementation

The overall control software consists of three different controllers, Experimental Controller (EC), Baseline Controller (BC), and Safety Controller (SC). A *controller* is a software module that implements a control algorithm to compute control commands. Different control algorithms are implemented in EC, BC and SC, and they are designed based on the concept of *analytical redundancy*. In the Simplex, the active controller is the controller whose control command is actually chosen to be sent to the physical system, and the application controllers refer to the control processes that are replaceable (e.g., the baseline controller and the experimental controller). For a detailed description of the Simplex and its structure in control systems, see Seto [Seto 98]. In this section, we discuss the design and implementation of the analytically redundant controllers.

Definition 1: Control algorithms are *analytically redundant with respect to a requirement R* if they generate control commands satisfying requirement R.

To apply Definition 3.1 to the design of EC, BC and SC, we need first to discuss the requirement that the control algorithms have to satisfy. Apparently, such a requirement is related to the control objective of the system. As we stated in the Introduction, the inverted pendulum is expected to be controlled to move from one track position to another while the pendulum is kept standing still at the upright position. Clearly, it is possible to try to stabilize the system at a new track position from anywhere on the track, but this scheme may lead to a failure of the system, such as the pendulum falling down or the cart running off the track as there are limitations on input voltage, track length, and cart velocity. To avoid such failures, we try to stabilize the system at a nearby track position and update the position towards the desired position periodically and at a predefined rate. The desired track position is referred to as a *target* and the generated nearby track positions are called *set points*. The set point generation can be done as part of the control algorithm, or be computed separately in a higher level control loop. It is the latter approach that we adopt in this report, which allows separation of concerns. In this multi-level control architecture, the lower level control will focus on stabilizing the system at a given set point, while the higher level control takes responsibility for generating proper set points which lead the physical system to the target. Let x_s and x_t be a set point and a target respectively. Then the control objectives for lower level controllers EC, BC and SC can be stated as *Stabilizing the system in Eq. (4) at $[x, \dot{x}, \theta, \dot{\theta}, I_a] = [x_s, 0, 0, 0, 0]$ subject to the constraints:*

$$|x| \leq 0.7, \quad |\dot{x}| \leq 1.0, \quad |\theta| \leq 30^\circ, \quad |V_a| \leq 4.96 \quad (5)$$

and the control objective for the higher level control: *Update the set point x_s every T seconds with the change vT until the generated set point reaches the target, i.e.,*

$$\begin{aligned} \text{while } (|x_s - x_t| > |vT|) \quad & x_s((k+1)T) = x_s(kT) + vT \\ \text{if } (|x_s - x_t| \leq |vT|) \quad & x_s((k+1)T) = x_t \end{aligned}$$

Where T is the sampling period of higher level control and v is the desired speed of the cart.

Remark 1: The control objective for higher level control can be considered as a trajectory generation for the cart. Namely, it generates a reference trajectory on track position for the system to follow. In this report, the reference trajectory is a linear function of time. It is not, however, the only possible reference.

With the control objective defined above, the lower level controllers EC, BC, and SC are said to be analytically redundant, with respect to stabilizing the physical system at a given set point, if all of them will stabilize the physical system at that set point. This definition implies that the control commands generated by EC, BC and SC could be different, but each one of them will stabilize the physical system at the given set point. Because of the constraints on state and control, the state space of the physical system, $[x, \dot{x}, \theta, \dot{\theta}]$, is divided to two exclusive regions, feasible region and unfeasible region. The feasible region is defined as a set that contains all the states of the physical system, satisfying all the state constraints. Apparently, any stability region of the physical system has to be a subset of the feasible region. To take into account the constraints, we modify the definition of analytically redundant controllers as: *the lower level controllers EC, BC and SC are said analytically redundant with respect to maintaining stability of the physical system in a given region if each one of the controllers will asymptotically stabilize the physical system inside the given region.* In this revised definition, we do not require the stability of the system to be guaranteed at a common set point. In fact, we say two controllers are analytically redundant if they both generate control commands within the control limits to asymptotically stabilize the physical system at some set point, which may not be the same, without violating the state constraints. We will require asymptotic stability to guarantee effective control of the cart position. While all the analytically redundant controllers will asymptotically stabilize the physical system, they may result in different system performance and stability region. In the rest of this section, we will investigate these differences and propose a design principle for the controllers.

3.1 Controller Design and System Performance

It is difficult, if not impossible, to design stabilization control algorithms and identify the corresponding stability regions for the nonlinear system in Eq. (4). Since our interest is to control the system in a neighborhood of an equilibrium state, it is reasonable to consider the linearization of the system at the equilibrium. In addition, since the variable I_a is not measurable,

and the inductance is relatively small ($L_a = 0.00018$ Henry), we reduce the order of the system by setting $L_a = 0$. This leads to

$$I_a = -\frac{K_g K_b}{r R_a} \dot{x} + \frac{1}{R_a} V_a$$

and

$$\begin{aligned}\ddot{x} &= \frac{1}{D} \left[\frac{1}{3} m l^2 (B_l V_a - f_c - C_1) + \frac{1}{2} m l \cos \theta (f_p + C_2) \right] \\ \ddot{\theta} &= \frac{1}{D} \left[-\frac{1}{2} m l \cos \theta (B_l V_a - f_c - C_1) - \bar{M} (f_p + C_2) \right]\end{aligned}$$

where

$$\bar{B} = \frac{K_g B_m}{r^2} + \frac{K_g^2 K_i K_b}{r^2 R_a}, B_l = \frac{K_g K_i}{r R_a}, C_1 = \bar{B} \dot{x} - \frac{1}{2} m l \sin \theta \dot{\theta}^2, C_2 = -\frac{1}{2} m g l \sin \theta$$

Furthermore, we drop the static friction terms by letting $A_x = A_\theta = 0$. Then the linearized system at $[x_s, 0, 0, 0]$ with x_s the set point is given by

$$\begin{bmatrix} \dot{x}_1 \\ \dot{x}_2 \\ \dot{x}_3 \\ \dot{x}_4 \end{bmatrix} = \begin{bmatrix} 0 & 1 & 0 & 0 \\ 0 & -a_{22} & -a_{23} & a_{24} \\ 0 & 0 & 0 & 1 \\ 0 & a_{42} & a_{43} & -a_{44} \end{bmatrix} \begin{bmatrix} x_1 \\ x_2 \\ x_3 \\ x_4 \end{bmatrix} + \begin{bmatrix} 0 \\ b_2 \\ 0 \\ -b_4 \end{bmatrix} V_a = AX + BV_a \quad (6)$$

where

$$\begin{aligned}X &= [x_1, x_2, x_3, x_4]^T = [x - x_s, \dot{x}, \theta, \dot{\theta}]^T, \quad D_l = 4\bar{M} - 3m, \\ a_{22} &= \frac{4\bar{B}}{D_l}, \quad a_{23} = \frac{3mg}{D_l}, \quad a_{24} = \frac{6B_\theta}{l D_l}, \quad b_2 = \frac{4B_l}{D_l}, \\ a_{42} &= \frac{6\bar{B}}{l D_l}, \quad a_{43} = \frac{6\bar{M}g}{l D_l}, \quad a_{44} = \frac{12\bar{M}B_\theta}{m l^2 D_l}, \quad b_4 = \frac{6B_l}{l D_l}\end{aligned}$$

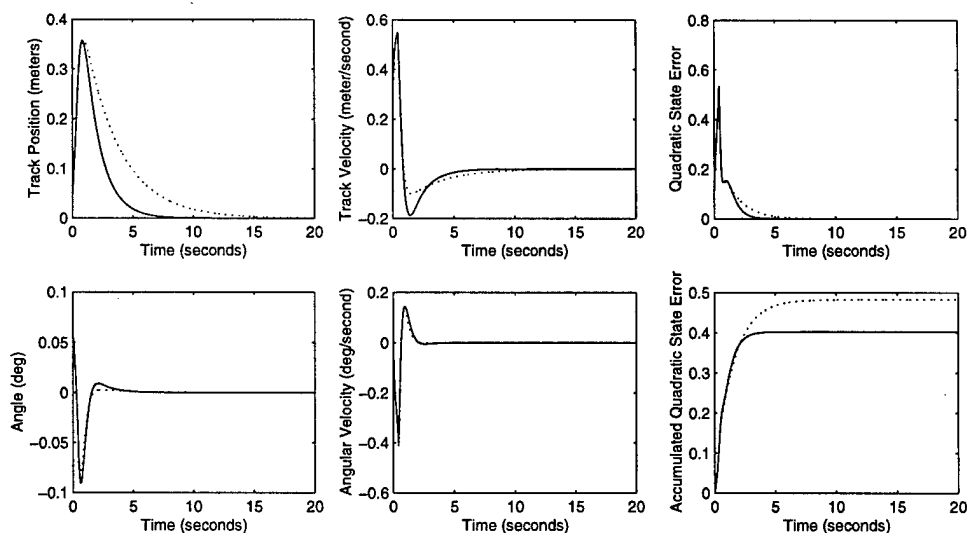
Design of the controllers EC, BC and SC will be based on the linearized model in Eq. (6). In this report, we will concentrate on linear state feedback control in the form $V_a = KX$, although other control synthesis may also be possible, especially for EC. To determine the control gain K , we solve the linear quadratic regulator (LQR) problem: find a control V_a such that the quadratic cost function $J(V_a) = \int_0^\infty (X^T D X + R V_a^2) dt$ is minimized, where D is a

4×4 symmetric and positive definite matrix and R is positive. The solution to this problem is given by a state feedback control law.

$$V_a = -R^{-1}B^T S X \quad (7)$$

where S is the solution of the Riccati equation $A^T S + SA - SBR^{-1}B^T S + D = 0$. It can be shown that, for each pair of D and R , there exists a unique solution S to the Riccati equation and a control law in Eq. (7) that asymptotically stabilizes the system in Eq. (6) at $X = 0$.

By varying matrix D and scalar R , the control gain obtained from them can be different, but all the resulting control algorithms will asymptotically stabilize the system at $X = 0$. The performance of the closed-loop system, however, may not be the same. For the inverted pendulum, we are interested in how good the controller is in terms of controlling the physical system to a set point and maintaining its stability there. Such a performance requirement is evaluated by the measures defined in Appendix A1. Namely, we will take a look at the overshoot, settling time and maximum deviation associated with the cart position, the settling time on quadratic state error, and the steady-state value of the accumulated quadratic state error. The following example illustrates the difference in performance caused by different controllers.



Solid Lines: results by V_{a1} ; Dotted lines: results by V_{a2}

Figure 4: Simulation Result

	V_{a1}	V_{a2}
Settling time (seconds)	7.66	15.76
Overshoot (meters)	0.0	0.0
Maximum derivation (meters)	0.36	0.36
Settling time on quadratic state error (seconds)	3.52	6.08
Steady-state value of the accumulated quadratic state error	0.40	0.48

Table 1: Performance Measures of the Closed-Loop System with V_{a1} and V_{a2}

Example 1: Linearized model of the inverted pendulum control system in Eq. (6), we design the stabilization control laws as in Eq. (7) by choosing two R s: $R = 0.01$ and $R=0.1$, and the same $D=\text{diag}(1,1,1,1)$. We will show that the control laws obtained from these different R s will cause different system performance. By running the Matlab, the LQR problem is solved with the control gains:

$$\begin{aligned} K_1 &= [10.0, 27.72, 103.36, 23.04] & \text{for } R = 0.01 \\ K_2 &= [3.16, 19.85, 69.92, 14.38] & \text{for } R = 0.1 \end{aligned}$$

Suppose the initial condition is chosen as $X_0 = [0.05, 0.31, 3.2 * \pi / 180, 0]$. Simulating the dynamics of the closed-loop system with control $V_{a1} = K_1 X$ and $V_{a2} = K_2 X$, we obtain the results summarized in Figure 4 and Table 1. From the performance measures, we conclude that the control V_{a1} results in a better performance than V_{a2} , while both controllers will stabilize the system at the equilibrium as indicated in Figure 4.

3.2 Stability Regions

While all the analytically redundant controllers stabilize the physical system at $X = 0$, they may result in different stability regions in addition to different system performance. It can be shown that the closed-loop system performance and the stability region are negatively related, i.e., the better performance of the closed-loop system performance is, the smaller the stability region will be. Generic analysis on such relation will be reported elsewhere, and in this report, we will demonstrate them with the inverted pendulum control system.

We first derive the safety region for a given controller. A stability region of the system in Eq. (6) under the control defined in Eq. (7) is a region in the state space of the physical system, from which the controller is able to asymptotically stabilize the physical system at $X = 0$ without violating any state or control constraints. We will focus on the stability regions described by a class of quadratic Lyapunov functions. Consider the constraints given by (5) in X -coordinate:

$$-0.7 - x_s \leq x_1 \leq 0.7 - x_s, \quad |x_2| \leq 1.0, \quad |x_3| \leq 30^\circ, \quad |KX| \leq 4.96$$

Obviously, the constraint on the cart position described above will be as the set point varies. Since the stability region is defined with respect to the equilibrium at a set point and is computed off-line, we would like the constraint on the cart position to be set with respect to the moving set point, i.e., $x_1 = x - x_s$ to be a constant. Since the total track range is $[-0.7, 0.7]$, and the eligible set point range is $[-0.5, 0.5]$, we restrict the cart motion in the range of $[-0.2, 0.2]$ from any given set point, i.e., $|x_1| \leq 0.2$. For the angle constraint, the current specification is too large, given that all the nonlinearities have been ignored in the linearized model. Hence we reduce the angle range by half. Then a revised feasible region Γ of the physical system is described by

$$\Gamma = \{X \mid |x_1| \leq 0.2, |x_2| \leq 1.0, |x_3| \leq 15^\circ, |KX| \leq 4.96\}$$

and a stability region S of the system in Eq. (7) with a given controller $V_a = KX$ is:

$$S = \{X \mid X^T P X \leq 1, P > 0, A^T P + P A < 0\} \subseteq \Gamma$$

Apparently, such a defined stability region is not unique for any given controller. To make a comparison on the stability regions between controllers, we consider the largest stability region as defined in Appendix A2. In particular, we first derive the largest stability region for a given controller, and then search the control gain K such that the resulting closed-loop system will have the largest stability region. The former is the case when K is known and the latter corresponds the case that K is known, which are both discussed in Appendix A2.

Case 1. K is given

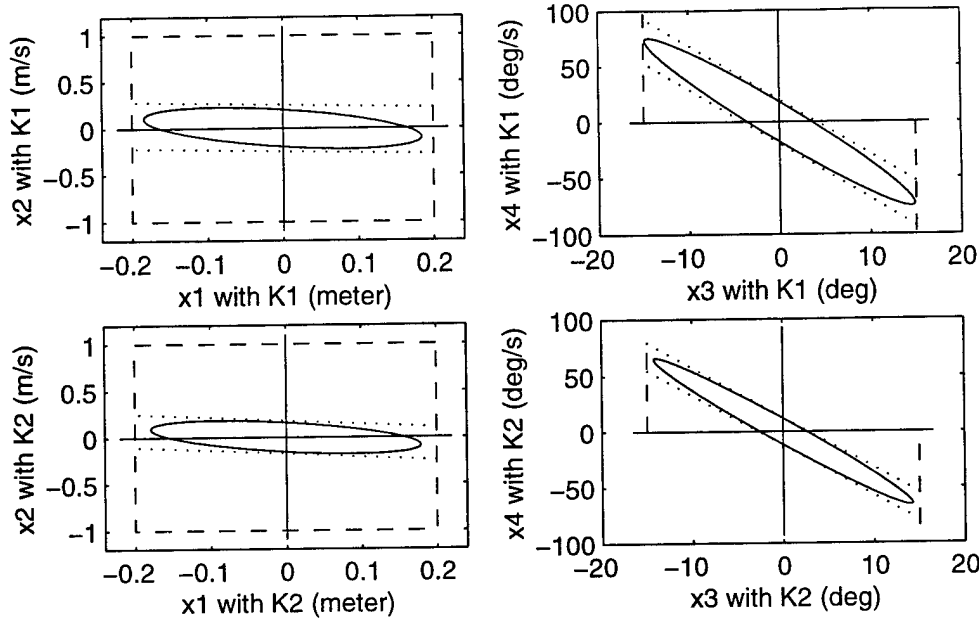
In this case, our objective is to identify the largest stability region inside the feasible region Γ for a given controller. The control gain has been obtained with other consideration, for instance, they could be chosen to satisfy some particular performance specifications. To find the largest stability region, we follow the procedure described in Appendix A2 and formulate the following LMI problem to determine matrix $Q = P^{-1}$:

$$\begin{aligned} &\text{minimize} \quad \log \det Q^{-1} \\ &\text{subject to} \quad QA^T + AQ < 0, \quad Q > 0 \\ &\quad \quad \quad a_k^T Q a_k \leq 1, \quad k = 1, \dots, 8, \end{aligned}$$

where

$$\begin{aligned} a_1 &= [5, 0, 0, 0]^T, & a_3 &= [0, 1, 0, 0]^T, & a_5 &= [0, 0, 3.82, 0]^T, & a_7 &= K / 4.95, \\ a_2 &= [-5, 0, 0, 0]^T, & a_4 &= [0, -1, 0, 0]^T, & a_6 &= [0, 0, -3.82, 0]^T, & a_8 &= -K / 4.95. \end{aligned}$$

This LMI problem is solved by the algorithm developed in Vandenberghe [Vandenberghe 98], and the resulting stability region, projected to $x_1 \sim x_2$ phase plan with $x_3 = x_4 = 0$ and $x_3 \sim x_4$ phase plane with $x_1 = x_2 = 0$, are shown in Figure 5.



Solid Lines: the boundary of the stability region;
Dashed Lines: the state constraints;
Dotted Lines: the constraints due to control limitation

*Figure 5: The Largest Stability Region
(with K_1 and K_2 projected to $x_1 \sim x_2$ phase plan and $x_3 \sim x_4$ phase plane)*

Case 2. K is unknown

In this case, we will find the best K , among all possible K s which render the physical system asymptotically stable, such that the corresponding controller will result in the largest stability region described by a quadratic Lyapunov function in the feasible region. Then the matrix $Q = P^{-1}$ can be determined by solving the following LMI problem:

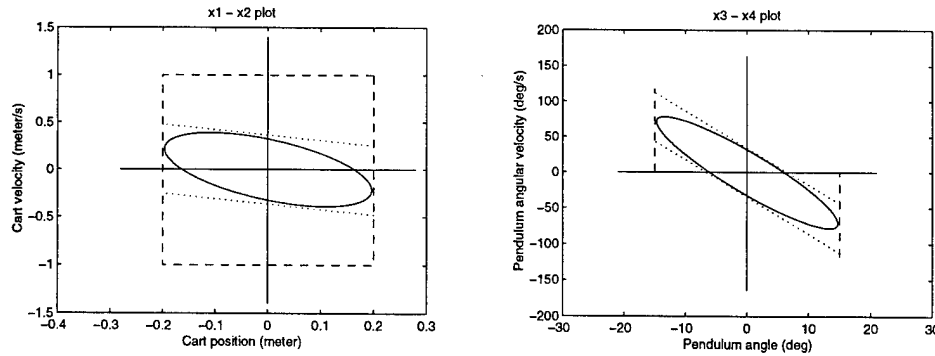
$$\begin{aligned}
&\text{minimize} && \log \det Q^{-1} \\
&\text{subject to} && QA^T + AQ + Z^T B^T + BZ < 0, \quad Q > 0 \\
& && a_k^T Q a_k \leq 1, \quad k = 1, \dots, 6 \\
& && \begin{bmatrix} I & b_j^T Z \\ Z^T b_j & Q \end{bmatrix} \geq 0, \quad j = 1, 2,
\end{aligned}$$

where

$$\begin{aligned}
a_1 &= [5, 0, 0, 0]^T, & a_3 &= [0, 1, 0, 0]^T, & a_5 &= [0, 0, 3.82, 0]^T, & b_1 &= 1/4.95, \\
a_2 &= [-5, 0, 0, 0]^T, & a_4 &= [0, -1, 0, 0]^T, & a_6 &= [0, 0, -3.82, 0]^T, & b_2 &= -1/4.95.
\end{aligned}$$

This problem again can be solved by the algorithm presented in [Vandenberghe 98]. The resulting stability region, projected to $x_1 \sim x_2$ phase plan with $x_3 = x_4 = 0$ and $x_3 \sim x_4$ phase plane

with $x_1 = x_2 = 0$, are shown in Figure 6. By solving K from equation $Z = KQ$, we obtain the control gain $K = [7.6, 13.54, 42.85, 8.25]$.



Solid Lines: the boundary of the stability region;
Dashed Lines: the state constraints;
Dotted Lines: the constraints due to control limitation

Figure 6: The Largest Stability Region
(with K variable, projected on $x_1 \sim x_2$ phase plan and $x_3 \sim x_4$ phase plane)

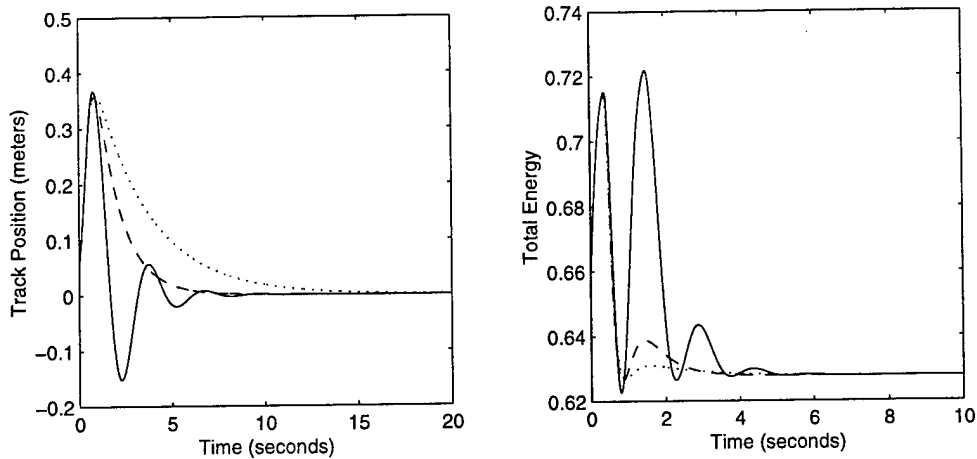
Finally, we conclude the controller design by comparing the performances and stability regions that different controllers result in. It is these differences that make the concept of analytic redundancy applicable. In all the cases, we have the control algorithm defined as a linear state feedback control in Eq. (7), but with the following control gains:

$$K_1 = [10.0, 27.72, 103.36, 23.04]$$

$$K_2 = [3.16, 19.85, 69.92, 14.38]$$

$$K_3 = [7.6, 13.54, 42.85, 8.25]$$

As discussed before, the controllers with K_1 and K_2 will yield different performance, while the controller with K_3 will result in the largest stability. Since the control gain K_3 is derived independent of the LQR approach, it will be inappropriate to consider its measures on quadratic state error used in LQR approach. Therefore, we compare the settling time and the energy. Figure 7 shows the performance measures of the closed-loop system; Figure 8 depicts the stability regions rendered by these controllers, and Table 2 summarizes the comparison. The stability regions are projected to $x_1 \sim x_2$ phase plan with $x_3 = x_4 = 0$ and $x_3 \sim x_4$ phase plane with $x_1 = x_2 = 0$, respectively.

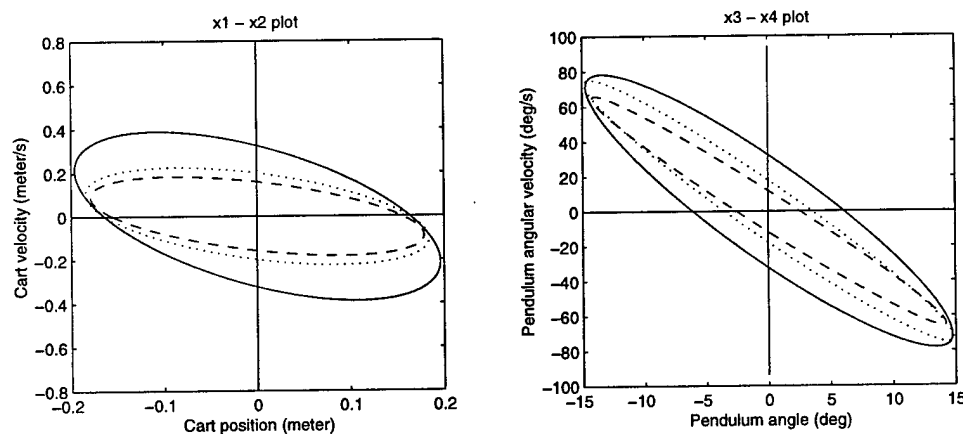


Dashed Lines: results corresponding to control K_1X ;

Dotted Lines: obtained with K_2X ;

Solid Lines: generated by K_3X

Figure 7: Performance Under Three Controllers



Dashed Lines: the results corresponding to control K_1X

Dotted lines: obtained with K_2X

Solid lines: generated by K_3X

Figure 8: The Largest Stability Regions
(projected to $x1 \sim x2$ phase plan and $x3 \sim x4$ phase plane)

	$K_1 X$	$K_2 X$	$K_3 X$
Settling time (seconds)	7.66	15.76	8.44
Overshoot (meters)	0.0	0.0	-0.152
Maximum derivation (meters)	0.36	0.36	0.37
Settling time on energy (seconds)	2.92	2.86	4.64
Measure of the size of stability region, ($\sqrt{\det Q}$)	0.0078	0.0144	0.0279

Table 2: Summary of the Comparison on Performance and Stability Region of Three Different Controllers

The above comparison shows that the controller with K_3 does give the largest stability region, but has the worst performance among all three controllers. On the other hand, the controller with gain K_1 yields a smallest safety region but has a much better performance. All three controllers are analytically redundant with respect to stabilizing the inverted pendulum at the equilibrium $X = 0$. Then the principle of controller design can be stated as: the control gain associated with a larger stability region should be used to construct a safety controller, while the control gain corresponding to better performance ought to be adopted for the baseline controller and the experimental controller.

3.3 Controller Implementation

In the inverted pendulum control system, the control algorithm for all the analytically redundant controllers are the same, namely, linear state feedback control $u = KX$ but with different control gains. These control gains are determined from solving LQR problems with the objective that the system performance under the baseline controller and the experimental controller will be satisfactory with respect to some performance specification, while the safety controller will offer the largest stability region among all these controllers. It is worth noting that the model that we use to compute the control gains is only an approximation of the real system, in which we have ignored all the nonlinearities, static frictions, motor dynamics, and other the uncertainties on dynamics and parameters. Therefore, the resulting control gains are expected to be off from the gains that should be actually used, and it is important to adjust them in experiments. Let K_b , K_e and K_s be the control gains for the baseline controller, the experimental controller and the safety controller, respectively. The following gains have been used for one inverted pendulum control system

$$K_b = [10.0, 36.0, 140.0, 14]; K_e = [8.0, 32.0, 120, 12]; K_s = [6.0, 20.0, 60.0, 16.0]$$

These controllers are implemented with a sampling frequency 50 Hertz.

In addition to model imprecision, the measurements of the track position and the pendulum angle are noisy are well. Since these are the only states can be measured from the physical system, the cart velocity and the pendulum angular velocity have to be constructed separately. Therefore, how to filter the measured data and construct the unknown states affect directly

the precision of the states that are used to compute the control command. From Figure 9, it is clear that the measurement noises¹ are above 5HZ. Hence a first-order digital Butterworth lowpass filter with cut-off frequency 5HZ is used. To construct the velocities, we apply the first order approximation, namely

$$\dot{x}(t) = [x(t) - x(t-T)]/T \text{ and } \dot{\theta}(t) = [\theta(t) - \theta(t-T)]/T$$

with T the sampling period. Although the position data in above construction are the results after filtering, they may still contain certain amount of noise. When the remaining noises are still relatively large, we extend the first order approximation over more periods to raise the signal-to-noise ratio. In those cases, we would have

$$\dot{x}(t) = [x(t) - x(t-mT)]/mT \text{ and } \dot{\theta}(t) = [\theta(t) - \theta(t-mT)]/mT$$

where m is an integer greater than one. Our experiments showed that, with $m = 2$, the constructed velocities are much more clean than the case when $m = 1$, but they suffer further delay. Therefore, the trade-off between clean velocity and the delay need to be carefully considered. For alternatives of velocity construction, one may consider using Kalman filter which eliminates the delay in data filtering and generates accurate velocity estimates simultaneously.

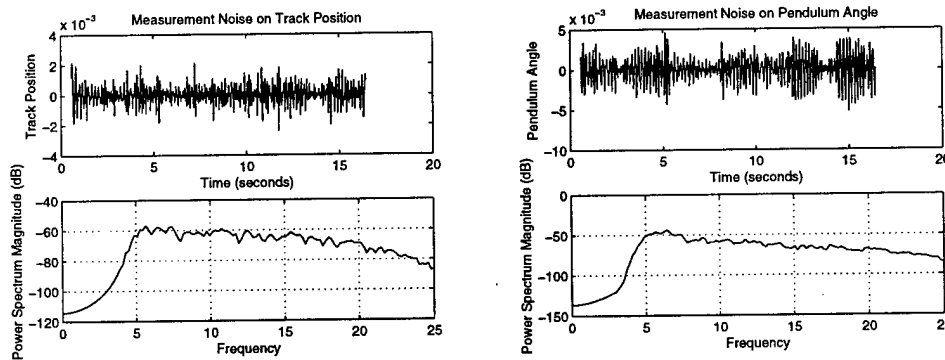


Figure 9: Measurement Noises of Track Position and Pendulum

Another practical issue in control implementation is delay. As we discussed in Appendix A4, a digital filter will cause delay. In fact, the lowpass digital filter that we used will cause 1-2 sampling periods delay. We will call such delay as *filtering delay*. While the effect of these delays can be compensated by adjusting the control gains in the control law, such delay will have a significant effect on safety checking of the system, as described in a later section. In addition to the filtering delay, the control implementation also causes one period delay. Spe-

¹ The noises shown are the difference between the physical measurements and the clean data. The clean data is obtained by filtering the raw data forwards and backwards using a high order lowpass filter, e.g., 10th order. While such filtering gives noiseless data with no delay, it can only be done off-line.

cifically, at each sample, the measured data is acquired and the computed control command is sent out. During one sampling period, for example, in $(t_0, t_0 + T)$, the control command $u(t_0 + T)$ is computed based on the state sampled at time t_0 , $x(t_0)$. This control will not be sent out to the physical system until the end of the period, i.e., $t_0 + T$.

At time $t_0 + T$, however, the state of the system has been evolved to $x(t_0 + T)$. Therefore, the control command will always act on the state that is one period later than the state from which the command was computed. We refer such type of delay as *digital implementation delay*. One may argue that the control command should be sent out right after it is computed, given that the computation of control command could be very short. While this arrangement can reduce the implementation delay, it may cause jittering and makes the scheduling of control tasks difficult if there are multiple tasks executing in a uniprocessor. We intentionally choose the implementation with one period delay to avoid jittering and to ease the schedulability analysis.

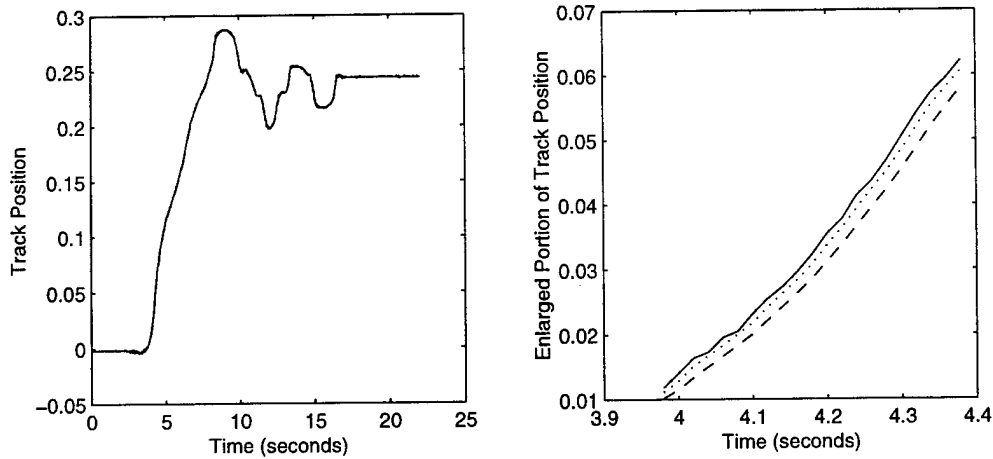
Both the filter delay and the digital implementation delay can be compensated by the model-based state projection, i.e., projecting state by solving the system equations. See Appendix A3 for detailed computation. Let $F = e^{AT}$, $G = \int_0^T e^{A\tau} d\tau$. Then the compensation of these delays in period $(t_0, t_0 + T)$ can be described as below.

Filtering delay compensation

Suppose there is one period filtering delay. Upon receiving the measurements from the physical system t_0 , we feed the data to the lowpass filter. Then the filtered data can be considered as the true (noiseless) track position and pendulum angle at the previous sample, i.e., $[x(t_0 - T), \theta(t_0 - T)]$. Constructing the velocities based on the filtered data, we obtain the full states at $t_0 - T$, $X(t_0 - T)$. Since the control command $u(t_0 - T)$ was output to the physical system at $t_0 - T$ and it acted on the state $X(t_0 - T)$, the full state at time t_0 can be projected as:

$$X(t_0) = FX(t_0 - T) + Gu(t_0 - T)$$

Figure 10 illustrates the filtering delay compensation by plotting the physical track position measured, filtered and projected, respectively, as the system is traveling from $x=0$ to $x=0.25$. We can see clearly from the enlarged portion, that the filtered data is delayed comparing to the raw measurement and the projected data compensates the delay.



Solid Lines: plot of the track position with the raw measurement

Dashed Lines: the filtered data

Dotted Lines: the projected data

Figure 10: Track Position with Raw Measurement, Filtered Data, and Projected Data

Digital implementation delay compensation

The control command $u(t_0)$ has been sent out to the physical system at time t_0 . The noiseless state of the physical system at t_0 is obtained from the compensation of the filtering delay. Then to find out at what state that the control command $u(t_0 + T)$ will start influencing the physical system, namely, what state that the physical system will be at the time $t_0 + T$ under the control $u(t_0)$, we project from $X(t_0)$ for one more period:

$$X(t_0 + T) = FX(t_0) + Gu(t_0)$$

This is the state at which the physical system will response to the control command $u(t_0 + T)$. Then we compute $u(t_0 + T)$ from the projected state $X(t_0 + T)$. While the digital implementation delay can be dealt with by model-based state projection, it is actually compensated for by adjusting the control gains properly in the experiments because the state feedback control is reasonably robust with respect to small delay. State projection will compensate for it in state safety checking discussed later.

4 Design of Control Switching Logic

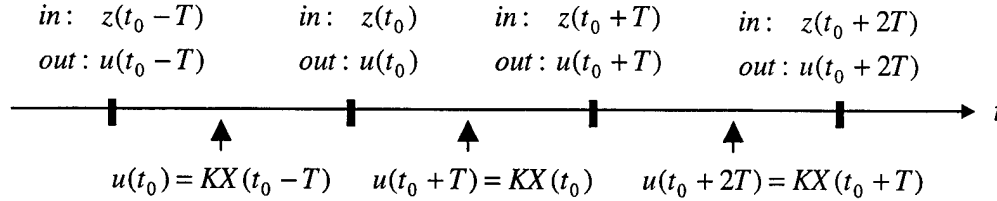
The control switching logic in the Simplex is designed to tolerate timing faults and semantic faults. It governs the selection of the active controller such that the safety controller will be chosen if a fault is detected, and the baseline controller will be in charge once the system is recovered from a faulty situation. To detect a timing fault, it is simply to check if the application controllers have missed their deadlines. For semantic fault, however, the detection is more involved. In the follows, we will first discuss an abstraction of the continuous dynamics of the physical system for semantic fault detection, and then design the control switching logic.

4.1 Safety Region and Safety of the Physical System

The analytically redundant controllers in the Simplex architecture will result in different stability regions. By evaluating the state of the physical system relative to the stability regions, control switches can be executed to tolerate the semantic faults. In particular, the safety controller is designed to provide safety protection, and therefore, the stability region of the safety controller is of special importance. In this section, we define the notion of the safety region and the safety criterion of the physical system, which will be used for the design of control switching.

A semantic fault is detected based on the behavior of the physical system. To abstract the continuous dynamics of the system, we define the safety region as the following: The *safety region with respect to the safety controller u_s* is defined as the largest stability region of the physical system under the control of u_s . Let P_s be the positive definite matrix which renders the stability region of the system to the largest. Then the safety region SR is given by $SR = \{X \mid X^T P_s X \leq 1\}$. A state X_0 is inside SR if $X_0^T P_s X_0 \leq 1$. Hence we would like to say that the physical system is safe if its state is inside the safety region, and for tolerating a semantic fault, we would design a switching logic to invoke the safety controller whenever the state of the physical system is out of the safety region. Such strategy, however, will not work. By the definition of stability region, it is clear that the physical system may not be stabilized if it starts from a state outside the stability region. Thus it would be too late for the safety controller to maintain system stability once the state of the physical system is out of its stability region. We refer this situation as the *safety region paradox*. To fix this problem, we need to know, at time t_0 , if the state of the physical system at t_0+T will be inside the safety region. If it is not, we would like to switch to the safety controller at t_0 . Given the filtering delay and digital implementation delay in the system, such a "look ahead" strategy can be extended as the following. Suppose (t_0, t_0+T) is the period that the control switching logic

needs to make a decision if the safety controller's output should be used. Let $z(t) = [x_m(t), \theta_m(t)]$ and $[x(t), \theta(t)]$ be the measurements and the noiseless data of the track position and the pendulum angle, respectively. Figure 11 shows the inputs from and outputs to the physical system.



Solid Lines: results by V_{a1} ;

Dotted Lines: results by V_{a2}

Figure 11: Simulation Result

Step 1. Filtering delay compensation

In this first step, the measurements $z(t_0)$ is obtained from the physical system. Following the compensation procedure described in last section, the true state of the physical system at time t_0 can be obtained from

$$X(t_0) = FX(t_0 - T) + Gu(t_0 - T)$$

Step 2. Digital implementation delay compensation

Again, as derived in last section, the state from which the physical system will response to the control command $u(t_0 + T)$ is given by

$$X(t_0 + T) = FX(t_0) + Gu(t_0)$$

Step 3. One more period projection to resolve the safety region paradox

If the safety controller were chosen as the active controller in the time interval $(t_0, t_0 + T)$, it would affect the physical system at $t_0 + T$. Therefore, the state $X(t_0 + T)$ can not be used to determine if the safety controller should be selected due to the safety region paradox. This implies that one more period state projection is needed. If the further projected state is out of the safety region, the safety controller will be switched to active and starts controlling the physical system at $t_0 + T$, at which the state of the physical system is still inside the safety region.

For this projection, we use the control command that is going to be sent out to the physical system. Let such control be $u(t_0 + T)$. Then the projection from $X(t_0 + T)$ under $u(t_0 + T)$ is given by

$$X(t_0 + 2T) = FX(t_0 + T) + Gu(t_0 + T)$$

Then the safety criterion of the physical system is given as: the physical system is safe the state $X(t_0 + 2T)$ is inside the safety region, i.e., $X(t_0 + 2T)^T P_s X(t_0 + 2T) \leq 1$; otherwise, it is unsafe. Let $P_b > 0$ be the matrix that gives the largest stability region of the physical system under the baseline control. We say that the physical system is ready for the baseline control if the state $X(t_0 + T)$ is inside the stability region given by P_b , i.e.

$X(t_0 + T)^T P_b X(t_0 + T) \leq 1$; otherwise, it is not ready. These are summarized in Figure 12.

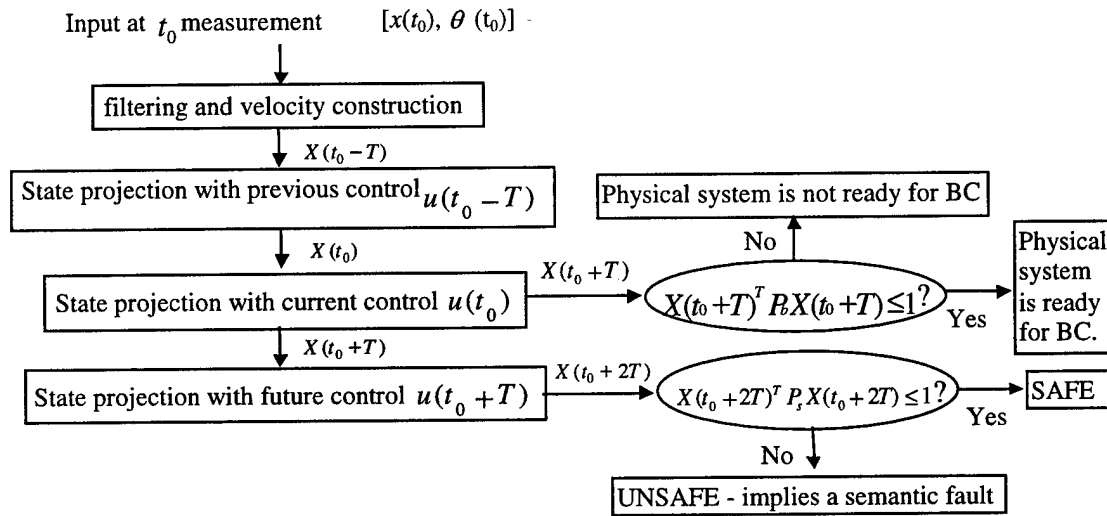


Figure 12: Check if the Physical System is Safe, and if it is Ready for Baseline Control

4.2 Design of Control Switching Logic

The control switching logic is designed based on the detection of timing fault and semantic fault. The former is simply to check if the application controllers have missed their deadlines, while the latter is to evaluate the state of the physical system with respect to the safety region. In addition to the behavior of the physical system and the timing performance of the application controllers, the user interface provides a way to manually affect the selection of the active controller by changing the availability of the application controllers. The state of an application controller is defined as follows:

Enabled	the controller is running and its output can be chosen to be sent to the physical system
Disabled	the controller is running but its output is disabled
Terminated	the controller is destroyed

When a controller is destroyed, all of the resources it has been allocated are released. For the inverted pendulum control system, the following assumptions have been imposed:

- When an application controller changes from being active to inactive because of a fault it contains, its output will be disabled until the user re-enables it.
- If both the experimental controller and the baseline controller are running with valid control commands, the experimental controller will be selected as the active controller.

The state transition of an application controller depends on the user's commands and if the controller changes from being active to inactive. In particular, the events that may cause a change of state of an application controller can be summarized in the set

{CREATE, DESTROY, ENABLE, DISABLE, A_TO_NA}

where CREATE/DESTROY and ENABLE/DISABLE are user's commands to start/terminate the process in which the controller is implemented, and to enable/disable the controller's output, respectively. A_TO_NA is the event when the controller is changed from being active to inactive. A state transition diagram is given in Figure 13.

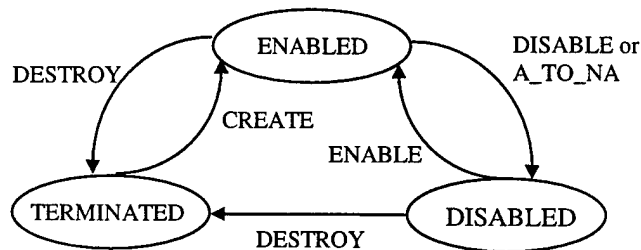


Figure 13: Application Controller State Transition Diagram

By combining the results of the availability of the application controllers, timing performance and the safety of the physical system, the control switching logic can be designed to tolerate timing and semantic faults. To represent the availability of an application controller and its timing performance, we define a Boolean variable *bc_ready* (*ec_ready*) for the baseline controller (experimental controller) as the following:

if BC meets its deadline AND it is enabled	if EC meets its deadline AND it is enabled
<i>bc_ready</i> = TRUE	<i>ec_ready</i> = TRUE
else	else
<i>bc_ready</i> = FALSE	<i>ec_ready</i> = FALSE

Suppose a control command with a value out of the allowable range (command invalid) is considered to be caused by a semantic fault in the controller. To describe the behavior of the physical system with relation to system safety and recovery from a faulty situation, define Boolean variables *safe* and *to_bc* with the following assignments:

if control output is valid AND the physical system is safe	if previous active controller is SC AND the physical system is ready for BC
<i>safe</i> = TRUE	<i>to_bc</i> = TRUE
else	else
<i>safe</i> = FALSE	<i>to_bc</i> = FALSE

Define the *state of the active controller* to be

{BASELINE, EXPERIMENTAL, SAFETY}

Then the state transition of the active controller will be determined by the values of the Boolean variables *bc_ready*, *ec_ready*, *safe* and *in_bc*. Figure 13 shows the state transitions of the active controller when the Boolean expressions on the transition arcs are TRUE.

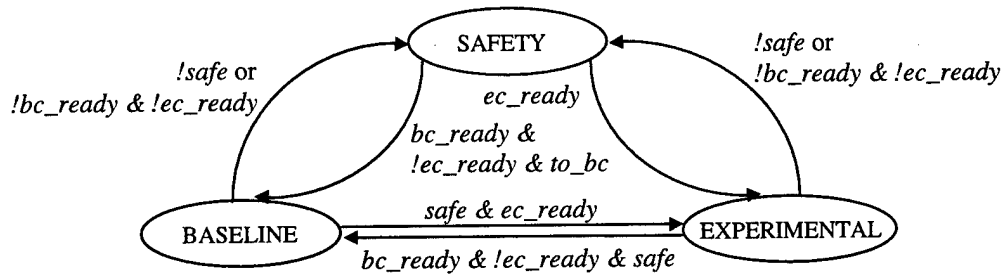


Figure 14: Active Controller State Transition Diagram

We have now completely established the control switching logic to determine the active controller. Implementation of this logic amounts to coding the state transition diagrams in Figures 13 and 14. To illustrate this control switching logic, we present the following example.

Example 2: Suppose the mission was to move the inverted pendulum from $x = -0.4$ to $x = 0.4$. All three controllers were running and the experimental controller initially controlled the system. A brute-force bug² was coded in the experimental controller and it triggered while the inverted pendulum was moving to the target. Upon detection of the bug, the active controller was switched to the safety control, and remained under safety control until the physical system was ready for the baseline control. Here we have used a reduced size safety region as the stability region of the baseline controller, namely, the region given by $\{X | X^T P_s X \leq 0.4\}$. To further reduce the effect of the noise on the value of Lyapunov function, we filtered the computed value of the Lyapunov function with a high order lowpass filter. The result was then

² An experimental controller with a brute-force generates the control command with the maximum (or minimum) control value allowed every sampling period.

used for the recovery check, a check to see if the physical system would be ready for the baseline control, i.e., if the filtered value is less than the threshold for recovery, 0.4. This delayed the switch to the baseline controller, but it guaranteed that the safety controller would not be switched back after the baseline controller was chosen to be the active controller.³

Figure 15 shows the trajectories of the physical system, and Figure 16 displays the results of safety checking and controller switches. As we can see from the figures, the experimental controller initially controlled the system, and it caused the system to behave badly after 11 seconds. At $t = 11.02$, the value of the Lyapunov function jumped over 1 and the bug was detected. At the same time, the safety controller was taking over the control. After one period since the safety controller was in charge, the value of the Lyapunov function dropped below 1, but the physical system was not ready for the baseline control yet. Having been controlled by the safety controller for four periods, the physical system became more stable, and the value of the Lyapunov function was reduced lower than 0.4. Hence at $t = 11.1$, the baseline controller was switched active, and remained in control afterwards.

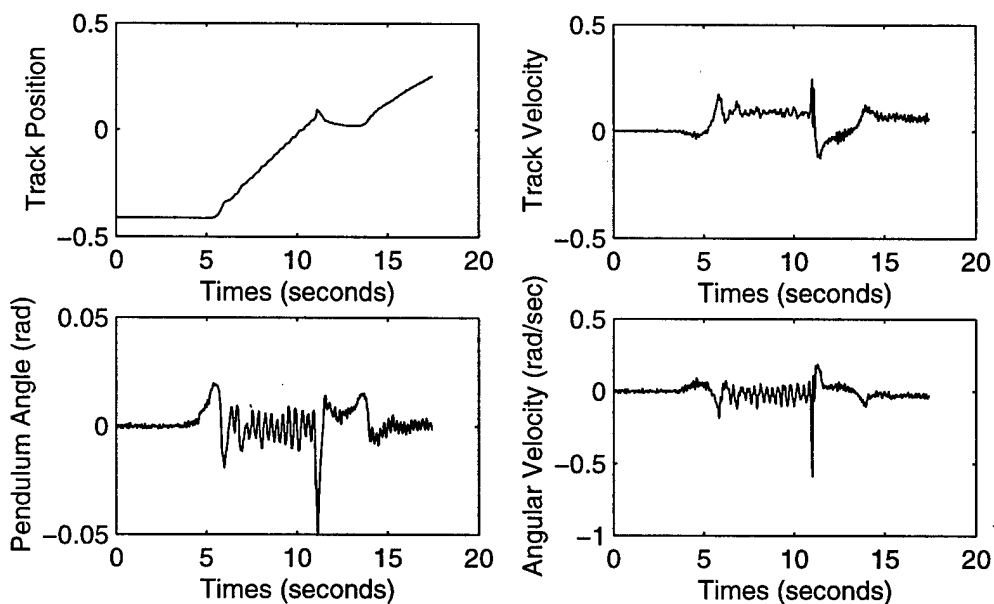


Figure 15: Illustration of Tolerating a Fault Caused by a Brute Force Bug

³ Theoretically, the value of the Lyapunov function should decrease monotonically under the safety controller, but it may not be the case in reality due to the measurement noise, the inaccuracy in system model and the construction of velocities. As a result, the value of the Lyapunov function can drop to a low level after the safety controller takes over control, which may trigger the switch to the baseline controller, and then bounce back to above 1 to knock out the baseline controller again.

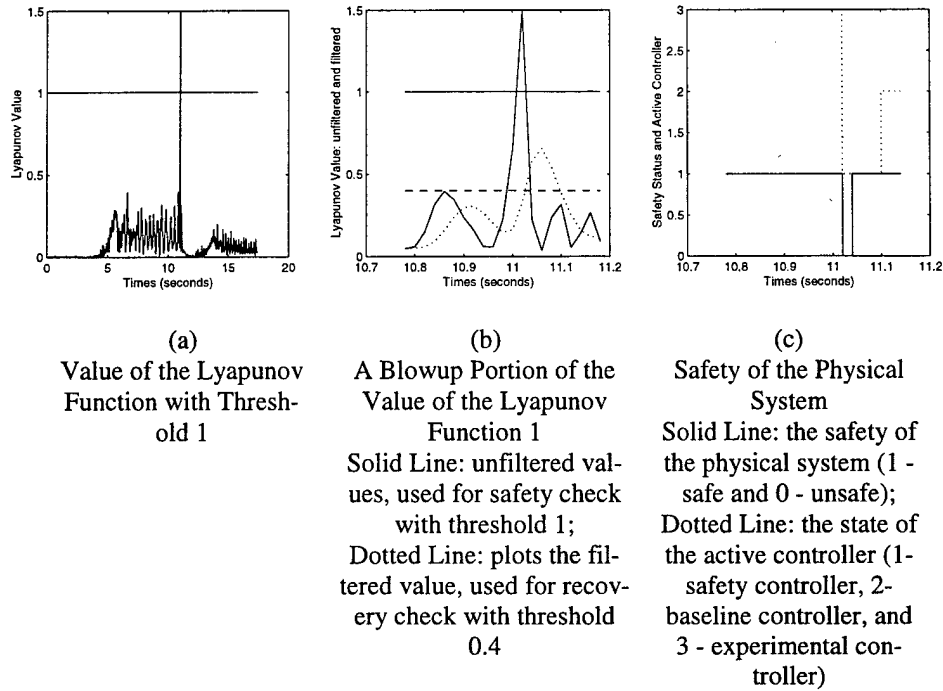


Figure 16: Lyapunov Function Values

5 Conclusions

In this report, we described analytical approaches for designing analytically redundant controllers, deriving the safety region, and establishing a control switching logic in an inverted pendulum control system using the Simplex. While these approaches were developed in association with a particular control system, the general analytic framework should be applicable to other control applications without much difficulty.

Analytic redundancy is the key concept in the Simplex architecture. Based on this concept, the baseline controller, the experimental controller, and the safety controller were designed as linear state feedback controls with the common requirement of asymptotically stabilizing the physical system at an given equilibrium state. While all of the controllers will achieve this goal, the closed-loop systems may have different performance in terms of the rate of convergence to the equilibrium and different stability regions. With certain well-defined performance measures, it can be shown that the performance of the closed-loop system is negatively related to the size of the corresponding stability region. Namely, the better performance the closed-loop system has, the smaller its stability region will be. It is this property that allows us to design the safety controller to render a large stability region although the performance it yields may not be superior, and the application controllers to focus on improving the performance while the stability regions they result in may be small. Such a combination enables an application controller to explore high functionality under the protection of the safety controller.

The safety region is defined as the largest stability region rendered by the safety controller. It is derived by solving a LMI problem subject to stability requirements as well as the state and control constraints. Two cases were considered: 1) derive the safety region for a given safety controller; and 2) design the safety controller such that the resulting safety region is maximized. In the latter case, the resulting stability region is the largest one described by a quadratic Lyapunov function among all possible linear state feedback controllers that asymptotically stabilize the physical system. For testing in the lab, we used the safety region derived with a given safety controller whose control gains have been adjusted in the real system for an acceptable performance.

The control switching logic was designed to tolerate the timing and semantic faults. It was established by taking into account the availability of the application controllers, the timing performance of the application controllers, and the safety of the physical system. The key step in the logic design is to correctly represent the state transition of the application controllers and the state transition of the active controller. While the specifications on fault tolerance

may vary from application to application, the basic structure of the state transition diagrams will remain the same, and design procedures can be carried over cross applications.

As the analytic approaches were employed in the real control system, there are practical/engineering issues need to be addressed. Many of them have occurred in our implementation, and we will discuss four of them here. First, the physical system needs to be well calibrated. The measurements of the track position and the pendulum angle are obtained from two potentiometers. After the A/D converter, the signals from the potentiometers are converted to digital ticks. Therefore, transformations from the ticks to the physical positions of the variables measured are needed. To derive such transformations, we manually move the cart to different locations on the track and fix the pendulum at different angles, and for each of these positions, record the tick readings. By applying least-square fitting, we found the linear relation between the physical position of the variable measured and the ticks read as in Figure 17.

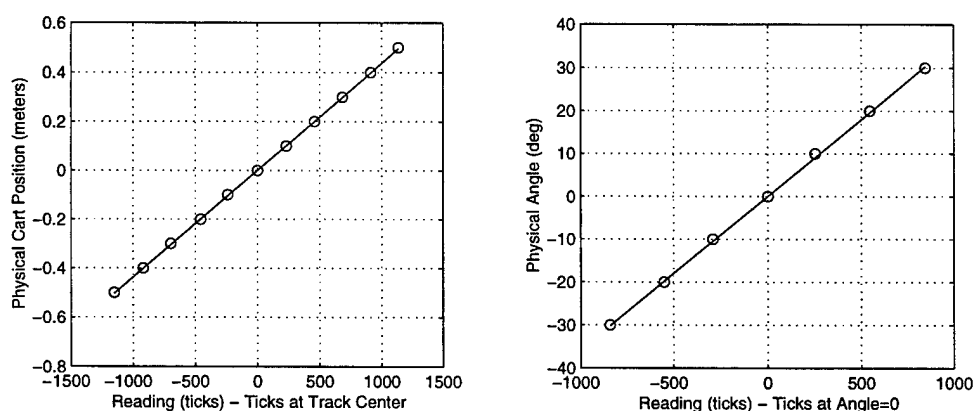


Figure 17: Linear Transformations Between the Physical Position of the Variable and the Ticks
*(cart position: $0.004365 * \text{ticks}$; angle: $0.0359 * \text{ticks}$)*

In addition to identifying the transformations, it is important to get the precise tick readings at the track center ($x = 0$) and zero angle ($\theta = 0$). These two measures may need to be recalibrated from time to time.

Second, the accuracy of the analytic model is important. As we have seen, both the model-based state projection and the derivation of the safety region are based on the analytic model. While the control algorithm is robust with respect to imprecision in the model, model-based state projection and the derived safety region could suffer significantly because of imprecision in the estimation of the run time system state and the model of the plant. The current model of the inverted pendulum was completely derived from mechanical principles, and some of its parameters were adjusted by comparing the simulation of the model and the results obtained from running the physical system. This guarantees the accuracy of the model in a short term, i.e., the matching results of simulation and the physical system trajectory in a

short time, say a few periods. For state projection in a longer time, we ought to carry through an extensive system identification procedure. This is certainly possible for a system like the inverted pendulum whose linearized model well represents the actual nonlinear system.

Third, the velocity construction plays an important role in both model-based state projection as well as the safety checking. When the state projection did not give a satisfactory result, the reason could be the inaccuracy of the model as we discussed above, but it is also possibly due to the approximation of velocities. As the position variables contain noise, the velocity approximation could be very poor. On the other hand, since the safety evaluation of the physical system depends on the calculation of a quadratic Lyapunov function, which involves the full states, the result obtained could be off significantly if the velocity components are poorly constructed. To resolve the velocity construction problem, the standard approach is to build an observer, or Kalman filter if noise is one of the issues need to be dealt with. Again this is a model-based methodology, and therefore, it would be better to use it in conjunction with a model identification approach, even though Kalman filter would tolerate a certain inaccuracy of the model. This is one of the subjects for further research.

Finally, in design of the safety controller, one objective is to make the corresponding stability region to be as large as possible, but this should not be pushed too far. As we discussed earlier, the larger the stability region is, the poorer the performance will be in the closed-loop system. In the inverted pendulum system, if the control gain is chosen such that the safety region is too large, the corresponding safety controller would take a longer time to drive the physical system to a neighborhood of the equilibrium state after it takes over the control from a faulty controller. Therefore, in the actual design, we need to make a trade-off between the volume gained and performance lost.

While the inverted pendulum is a prototype system, it certainly contains a lot of control issues. We would like to emphasize that the analytic approaches developed to address these issues can be very well extended to other control applications, including large-scale control systems. On the other hand, of course, there are still some unsolved problems and they will be investigated in our future research.

References

- [Boyd 94]** Boyd, S.; El Ghaoui, L.; Feron, E.; & Balakrishnan, V. "Linear Matrix Inequalities in System and Control Theory." *SIAM Studies in Applied Mathematics*. Philadelphia, PA: Society for Industrial and Applied Mathematics (SIAM), 1994.
- [Vandenberghe 98]** Vandenberghe, L.; Boyd, S.; & Wu, S.P. "Determinant Maximization with Linear Matrix Inequality Constraints." *SIAM Journal on Matrix Analysis and Application* Vol. 19 (1998).
- [Seto 98]** Seto, D.; Krogh, B.H.; Sha, L.; & Chutinan, A. "The Simplex Architecture for Safe On-line Control System Upgrades." *IEEE Control System Magazine* (August 1998).

Appendix A

A1 Performance Evaluation

Consider a linear time-invariant system (LTI)

$$\dot{X} = AX + Bu$$

where $X \in R^n, u \in R^m, A \in R^{n \times n}, B \in R^{n \times m}$. u is the linear state feedback control designed to minimize the quadratic cost $J(u) = \int_0^\infty (X^T Q X + u^T R u) dt$, where Q and R are positive definite. Then the performance of the closed-loop system can be evaluated by system transient response, settling time on quadratic state error, steady-state of the accumulated quadratic state error, and settling time on energy, which are defined as the follows.

Transient Response of A State Variable Let $x(t)$ be the dynamic variable under study and x_s be the set point for $x(t)$ to reach. Then the transient response of $x(t)$ is measured by the overshoot O_s , the settling time S_t , and the maximum deviation D_m , defined as the follows. Figure 18 illustrates these measures.

$$\text{overshoot of } x(t): \begin{cases} \text{when } x(t_0) < x_s, O_s = \begin{cases} \max_{t \geq t_0} (x(t)) - x_s & \text{if } \max_{t \geq t_0} (x(t)) > x_s \\ 0 & \text{otherwise} \end{cases} \\ \text{when } x(t_0) > x_s, O_s = \begin{cases} x_s - \min_{t \geq t_0} (x(t)) & \text{if } \min_{t \geq t_0} (x(t)) < x_s \\ 0 & \text{otherwise} \end{cases} \\ \text{when } x(t_0) = x_s, O_s = \max_{t \geq t_0} |x(t) - x_s| \end{cases}$$

settling time of $x(t)$: $S_t = t_1 - t_0$ where t_1 is the smallest t such that $\forall t > t_1$

$$\begin{cases} |x(t) - x_s| \leq 0.05 |x(t_0) - x_s| & x(t_0) \neq x_s \\ |x(t) - x_s| \leq 0.05 \max_{t \geq t_0} |x(t) - x_s| & x(t_0) = x_s \end{cases}$$

$$\text{maximum deviation: } D_m = \max_{t \geq t_0} |x(t) - x_s|$$

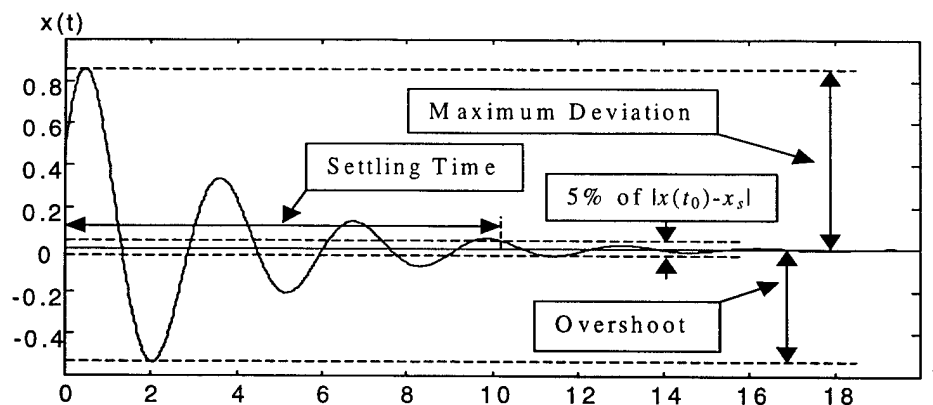


Figure 18: Measures for the Transient Response of $x(t)$

Settling Time on Quadratic State Error

By quadratic state error, it is meant the quadratic term of state variables in the cost function, i.e., $E_x(t) = X^T(t)QX(t)$. Then the *settling time on quadratic state error* is defined as the time $t_1 - t_0$ with t_0 being the time when the quadratic state error decreases to 5% of $E(t_0)$ and stay within that range for all $t > t_1$.

Steady-State Value of the Accumulated Quadratic State Error

It can be shown that the quadratic cost $J(u)$ is bounded when the closed-loop system is asymptotically stable. Therefore, the *steady-state of the accumulated quadratic state error* is defined as

$$\overline{E_x} = \int_{t_0}^{\infty} X^T(t)QX(t)dt$$

Settling Time on Energy

As described in Section 2, the total energy of the inverted pendulum system is given by

$$E(t) = \frac{1}{2}(M + m)\dot{x}(t)^2 + \frac{1}{2}ml \cos \theta \dot{\theta}(t)^2 + \frac{1}{6}ml^2 \dot{\theta}(t)^2 + \frac{1}{2}mgl \cos \theta(t)$$

For an asymptotically stable closed-loop system, the total energy of the system will tend to the constant value $E_e = \frac{1}{2}mgl$, which is the potential energy of the system when the pendulum is at the upright position. Then the settling time on energy is defined as $S_{te} = t_{1e} - t_0$ where t_{1e} is the smallest t such that $\forall t > t_{1e}$

$$\begin{cases} |E(t) - E_e| \leq 0.05 |E(t_0) - E_e| & E(t_0) \neq E_e \\ |E(t) - E_e| \leq 0.05 \max_{t \geq t_0} |E(t) - E_e| & E(t_0) = E_e \end{cases}$$

A2 Stability Region of Linear Control Systems with Linear Constraints

The stability region of a linear control system will be restricted by the constraints imposed to the system. The system can only evolve in the feasible region in the state space, where no constraints will be violated. Thus, a stability region has to be a subset of the feasible region. Consider a linear control system:

$$\dot{X} = AX + Bu \text{ with constraints: } a_k^T X \leq 1, \quad k = 1, \dots, q \text{ and } b_j^T u \leq 1, \quad j = 1, \dots, r,$$

where $X \in R^n$, $u \in R^m$, $a_k \in R^n$ and $b_j \in R^m$ are constant vectors. The stabilization control algorithm is a linear state feedback control given by $u = KX$. Then the closed-loop system becomes time-invariant and the constraints on control variables can be expressed in terms of the state variables, i.e.,

$$\dot{X} = \bar{A}X \text{ with constraints: } \alpha_k^T X \leq 1, \quad k = 1, \dots, p \quad (A1)$$

where $\bar{A} = A + BK$, $\alpha_i = a_i$, $\alpha_{q+j} = b_j^T K$, $i = 1, \dots, q$, $j = 1, \dots, r$, and $p = q + r$. Then the objective is to find the control gain K such that the closed-loop system is asymptotically stable. Clearly, there are infinite many K s will do the work as long as all the eigenvalues of the resulting matrix \bar{A} are in the left half of the complex plan. To establish the relation between the choice of K and the stability region associated with the control using K as the control gain, we apply Lyapunov stability analysis.

Definition A1: The system in Eq. (A1) is *quadratically stable* if there exists a positive definite matrix $P > 0$ such that the quadratic function $V(X) = X^T P X$ has negative derivatives along all the trajectories of (A1).

The Lyapunov stability criterion states that *the system in Eq. (A1) is asymptotically stable if and only if it is quadratically stable*. Hence it is sufficient to study quadratic Lyapunov function for the stability analysis of the system in Eq. (A1). Since

$$\dot{V} = X^T (\bar{A}^T P + P \bar{A}) X$$

along the trajectories of Eq. (A1), we conclude that the system in Eq. (A1) is asymptotically stable if and only if there exist a matrix P such that

$$P > 0, \quad \bar{A}^T P + P \bar{A} < 0 \quad \text{or} \quad Q = P^{-1} > 0, \quad Q \bar{A}^T + \bar{A} Q < 0 \quad (\text{A2})$$

Then a stability region S of Eq. (A1) can be defined as $S = \{X \mid X^T P X \leq 1\}$. Apparently, any stability region has to satisfy the constraints, namely, every point inside the region satisfies the constraints. The following result establishes the conditions for S to satisfy the constraints.

Lemma A1: Given a LTI system with constraints in Eq. (A1). The stability region S of Eq. (A1) satisfies the constraints in (A1) if and only if $\alpha_k^T P^{-1} \alpha_k \leq 1, k = 1, \dots, p$.

Proof: By definition, S satisfies the constraints if and only if $\alpha_k^T X \leq 1 \quad \forall X \in S, k = 1, \dots, p$.

This implies that S satisfies the constraints if and only if

$$\max_{X \in S} \alpha_k^T X \leq 1, k = 1, \dots, p \Leftrightarrow \alpha_k^T P^{-1} \alpha_k \leq 1, k = 1, \dots, p.$$

Next we will show $\max_{X \in S} \alpha_k^T X = \sqrt{\alpha_k^T P^{-1} \alpha_k}, \quad \forall k = 1, \dots, p$, which implies the latter condition.

To this end, we solve the following nonlinear programming problem for each $k=1, \dots, p$:

$$\begin{aligned} & \text{maximize } \alpha_k^T X \\ & \text{subject to } X^T P X \leq 1 \end{aligned}$$

Let X^* be the optimal solution. Then Kuhn-Tucker conditions are satisfied, namely

$$\begin{cases} \alpha_k^T - 2\lambda X^{*T} P = 0 \\ \lambda(1 - X^{*T} P X^*) = 0 \\ \lambda \geq 0 \end{cases}$$

Apparently, there is a solution only if $\lambda > 0$. Solving above equations, we obtain

$$X^* = (P^{-1})^T \alpha_k / \sqrt{\alpha_k^T P^{-1} \alpha_k} \Rightarrow \max_{X \in S} \alpha_k^T X = \sqrt{\alpha_k^T P^{-1} \alpha_k}$$

Then we conclude that $\max_{X \in S} \alpha_k^T X \leq 1$ if and only if $\alpha_k^T P^{-1} \alpha_k \leq 1$ for all $k=1, \dots, p$.

Given that the stability region is not unique, we are interested in deriving the largest S subject to the constraints. Since each stability region defines an ellipsoid geometrically in the state space of the system, by the size of a stability region, it is meant the volume of the ellipsoid. Maximizing the size of a stability region is carried out by formulating a linear matrix inequality (LMI) problem, which is described extensively in [Boyd 94]. We consider two different cases. First, control gain K is given. By solving a LQR problem, a control gain K is obtained such that the closed-loop system is asymptotically stable. In this case, the system in

Eq. (A1) is completely determined, and the objective is to find a matrix P such that the size of S is the largest subject to constraints and conditions in (A2). Second, control gain K is unknown. Then we need to determine matrix P and K to maximize the size of S and subject to conditions in (A2) and those given as constraints. The resulting stability region in this case will be the largest one given by quadratic Lyapunov functions among all possible K s which render the physical system asymptotically stable. We discuss these two cases separately as follows.

Case 1. When K is given

In this case, matrix \bar{A} is completely determined. Since the volume of an ellipsoid given by $S = \{X | X^T P X \leq 1\}$ is proportional to $\sqrt{\det P^{-1}}$, then the problem of maximizing the volume subject to constraints can be formulated as a LMI problem:

$$\begin{aligned} & \text{minimize} \quad \log \det Q^{-1} \\ & \text{subject to} \quad Q \bar{A}^T + \bar{A} Q < 0, \quad Q > 0 \\ & \quad \quad \alpha_k^T Q a_k \leq 1, \quad k = 1, \dots, p \end{aligned}$$

This problem is solved by Vandenberg et al. in [Vandenberghe 98].

Case 2. When K is unknown In this case, K needs to be determined along with matrix P to guarantee asymptotic stability of the system and the largest stability region, subject to constraints. By substituting $\bar{A} = A + BK$ in the derivatives of V , we obtain the condition:

$$QA^T + AQ + QK^T B^T + BKQ < 0$$

By introducing the change of variable $Z = KQ$, above condition becomes

$$QA^T + AQ + Z^T B^T + BZ < 0$$

and the constraints

$$b_j^T u \leq 1 \Rightarrow b_j^T K Q K^T b_j \leq 1 \Rightarrow b_j^T Z Q^{-1} Z^T b_j \Rightarrow \begin{bmatrix} I & b_j^T Z \\ Z^T b_j & Q \end{bmatrix} \leq 1, \quad j = 1, \dots, r$$

where the first step is the result of Lemma (A1), the second step is due to the change of variable, and the last step is carried out by Schur complements. Then the LMI problem can be formulated as:

$$\begin{aligned}
& \text{minimize} \quad \log \det Q^{-1} \\
& \text{subject to} \quad QA^T + AQ + Z^T B^T + BZ < 0, \quad Q > 0 \\
& \quad \quad \quad a_k^T Q a_k \leq 1, \quad k = 1, \dots, q \\
& \quad \quad \quad \begin{bmatrix} I & b_j^T Z \\ Z^T b_j & Q \end{bmatrix} \geq 0, \quad j = 1, \dots, r
\end{aligned}$$

Again, this problem can be solved by the approach developed in [Vandenberghe 98].

A3 Digitized Control Implementation

Consider a linear system

$$\dot{x} = Ax + Bu, \quad y = Cx$$

where $x \in R^n, u \in R^m, y \in R^p, A \in R^{n \times n}, B \in R^{n \times m}, C \in R^{p \times n}$. Then the trajectory of the system, starting from x_0 at t_0 , is given by:

$$x(t) = e^{A(t-t_0)} x(t_0) + \int_{t_0}^t e^{A(t-\tau)} Bu(\tau) d\tau$$

Let $t_0 = kT, t = (k+1)T$, with T the sampling period. Since the control $u(t) = u(kT)$ for all $kT \leq t < (k+1)T$, x at $(k+1)T$ is derived as:

$$x((k+1)T) = e^{AT} x(kT) + \left(\int_{kT}^{(k+1)T} e^{A((k+1)T-\tau)} d\tau \right) Bu(kT) = Fx(kT) + Gu(kT)$$

with $F = e^{AT}, G = \int_0^T e^{A(T-\tau)} d\tau$. Suppose a linear state feedback control is designed as in the simple form $u(t) = Kx(t)$, then the digitized state feedback control system is given by

$$x((k+1)T) = (F + GK)x(kT)$$

A4 Delay Caused by Digital Filter

A digital filter can be described as

$$a_0 y(n) = b_0 + \sum_{k=1}^{n_b} b_k x(n-k) - \sum_{k=1}^{n_a} a_k y(n-k)$$

with $x(\bullet)$ and $y(\bullet)$ the raw data and filtered data, respectively. Design of a digital filter can be carried out directly from digital design by using certain commercially available software package, for example, Matlab Signal Processing toolbox, or from a design of analog filter.

Digital Design

By making use of Matlab, a digital filter is designed with the coefficients a_k and b_k as

$$H(z) = \frac{\sum_{k=0}^{n_b} b_k z^{-k}}{\sum_{k=0}^{n_a} a_k z^{-k}} \text{ and frequency response: } H(e^{j\omega}) = \frac{\sum_{k=0}^{n_b} b_k e^{-jk\omega}}{\sum_{k=0}^{n_a} a_k e^{-jk\omega}}$$

Let

$$B_r = \sum_{k=0}^{n_b} b_k \cos k\omega, \quad B_i = \sum_{k=0}^{n_b} b_k \sin k\omega, \quad A_r = \sum_{k=0}^{n_a} a_k \cos k\omega, \quad A_i = \sum_{k=0}^{n_a} a_k \sin k\omega$$

Then the frequency response can be written as

$$H(e^{j\omega}) = H_r + jH_i \quad \text{with} \quad H_r = \frac{B_r A_r + B_i A_i}{A_r^2 + A_i^2}, \quad H_i = \frac{B_r A_i - B_i A_r}{A_r^2 + A_i^2}$$

Let f and T be the sampling frequency and period. With $\omega = 2\pi(f_s/f)$, the delay D caused by the digital filter at frequency f_s can be computed as

$$D = (\angle H(e^{j\omega})/2\pi)/f_s \text{ (seconds)} \quad \text{or} \quad D = ((\angle H(e^{j\omega})/2\pi)/f_s)/T \text{ (sampling periods)}$$

Analog Design and Digitization

Let f be the sampling frequency and T be the sampling period. A digital filter can be designed from an analog filter by applying the bilinear transformation:

$$s = \frac{2}{T} \frac{1 - z^{-1}}{1 + z^{-1}}$$

Suppose an analog filter is given by transfer function $H(s)$. Then a digital filter can be obtained from this analog filter with the frequency response

$$H(e^{j\omega}) = H(s) \Big|_{s = \frac{2}{T} \frac{1 - e^{-j\omega}}{1 + e^{-j\omega}}}$$

and the delay caused by the filtering can be computed as described before.

Example A1. Consider a first order Butterworth lowpass filter with cut-off frequency $f_c = 5\text{HZ}$ and sampling frequency $f = 50\text{HZ}$. By running the Matlab, we obtain the filter

coefficients $a_0 = 1$, $a_1 = -0.5095$, $b_0 = b_1 = 0.2452$. Then the magnitude response and the phase response are given by

$$|H(e^{j\omega})| = \frac{2b_1}{\sqrt{(1+a_1)^2 + (1-a_1)^2 \tan^2(\omega/2)}}, \quad \angle H(e^{j\omega}) = -\tan^{-1} \frac{(1-a_1) \tan(\omega/2)}{(1+a_1)}$$

Figure 19(a) shows the delay as a function of the signal frequency. For instance, the delay of a signal with frequency $f_s = 4.1\text{HZ}$ is 1.324 sampling periods, namely, 1-2 sampling periods in implementation. This is verified by the plot in Figure 19(b) where the time lag between the first perks of the signal and the filtered signal is 20 ms and the lag for the second perks is 40 ms.

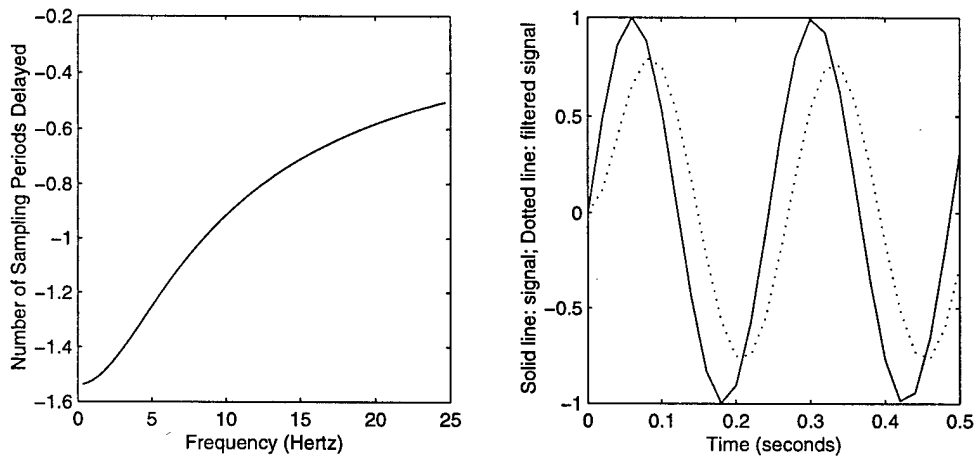


Figure 19: (a) Number of Sampling Periods Delayed as a Function of the Signal Frequency
(b) Signals Before and After Filtering

REPORT DOCUMENTATION PAGE			Form Approved OMB No. 0704-0188	
Public reporting burden for this collection of information is estimated to average 1 hour per response, including the time for reviewing instructions, searching existing data sources, gathering and maintaining the data needed, and completing and reviewing the collection of information. Send comments regarding this burden estimate or any other aspect of this collection of information, including suggestions for reducing this burden, to Washington Headquarters Services, Directorate for Information Operations and Reports, 1215 Jefferson Davis Highway, Suite 1204, Arlington, VA 22202-4302, and to the Office of Management and Budget, Paperwork Reduction Project (0704-0188), Washington, DC 20503.				
1. AGENCY USE ONLY (LEAVE BLANK)		2. REPORT DATE November 1999		3. REPORT TYPE AND DATES COVERED Final
4. TITLE A Case Study on Analytical Analysis of the Inverted Pendulum Real-Time Control System			5. FUNDING NUMBERS C — F19628-95-C-0003	
6. AUTHOR(S) Seto, Danbing Sha, Lui				
7. PERFORMING ORGANIZATION NAME(S) AND ADDRESS(ES) Software Engineering Institute Carnegie Mellon University Pittsburgh, PA 15213			8. PERFORMING ORGANIZATION REPORT NUMBER CMU/SEI-99-TR-023	
9. SPONSORING/MONITORING AGENCY NAME(S) AND ADDRESS(ES) HQ ESC/DIB 5 Eglin Street Hanscom AFB, MA 01731-2116			10. SPONSORING/MONITORING AGENCY REPORT NUMBER	
11. SUPPLEMENTARY NOTES				
12.A DISTRIBUTION/AVAILABILITY STATEMENT Unclassified/Unlimited, DTIC, NTIS			12.B DISTRIBUTION CODE	
13. ABSTRACT (MAXIMUM 200 WORDS) An inverted pendulum has been used as the controlled device in a prototype real-time control system employing the Simplex™ architecture. In this report, we address the control issues of such a system in an analytic way. In particular, an analytic model of the system is derived; control algorithms are designed for the baseline control, experimental control and safety control based on the concept of analytic redundancy; the safety region is obtained as the stability region of the system under the safety control; and the control switching logic is established to provide fault tolerant functionality. Finally, the results obtained and the lessons learned are summarized, and future work is discussed.				
14. SUBJECT TERMS analytic redundancy, fault tolerance, linear matrix inequality, Lyapunov function, real-time control, Simplex architecture			15. NUMBER OF PAGES 42 pp.	
			16. PRICE CODE	
17. SECURITY CLASSIFICATION OF REPORT UNCLASSIFIED	18. SECURITY CLASSIFICATION OF THIS PAGE UNCLASSIFIED	19. SECURITY CLASSIFICATION OF ABSTRACT UNCLASSIFIED	20. LIMITATION OF ABSTRACT UL	